IEEE Access
Multidisciplinary ⋮ Rapid Review ⋮ Open Access Journal

Received March 22, 2020, accepted April 28, 2020, date of publication May 6, 2020, date of current version May 20, 2020.

Digital Object Identifier 10.1109/ACCESS.2020.2992674

Highly Repeatable Rope Winch Design With Multiple Windings and Differential Gear Mechanism

SUNGKEUN YOO[1], TAEGYUN KIM[2], MYOUNGJAE SEO[3], JOOHYUN OH[3], JONGWON KIM[1], HWA SOO KIM[4], (Member, IEEE), AND TAEWON SEO[3], (Member, IEEE)

[1]School of Mechanical and Aerospace Engineering, Seoul National University, Seoul 08826, South Korea
[2]School of Mechanical Engineering, Yeungnam University, Gyeongsan 38541, South Korea
[3]School of Mechanical Engineering, Hanyang University, Seoul 04763, South Korea
[4]Department of Mechanical System Engineering, Kyonggi University, Suwon 16227, South Korea

Corresponding authors: Hwa Soo Kim (hskim94@kgu.ac.kr) and Taewon Seo (taewonseo@hanyang.ac.kr)

This research was supported in part by the National Research Foundation of Korea (NRF) Grant funded by the Ministry of Science and ICT for First-Mover Program for Accelerating Disruptive Technology Development (2018M3C1B9088331, 2018M3C1B9088332), and in part by the National Research Foundation of Korea Grant funded by the Korea Government (Ministry of Science and ICT) under Grant 2019R1G1A1100785.

ABSTRACT This paper presents a rope winch with high position repeatability using a differential gear mechanism. This winch is easy to apply to existing buildings using synthetic fiber ropes, which are generally used by building exterior maintenance workers, and can be widely utilized as a winch of a gondola or climbing robot. Multiple pulleys are used to achieve high payloads, and differential gear mechanisms are used to distribute the torque across each pulley evenly. Uniform torque distribution minimizes slipping on each pulley, which reduces the power loss due to friction. This is proven through an analysis using the capstan equation and an experiment on a test bench. In addition, a criterion for the position repeatability of the winch is designed, and its results show that one pressure roller achieves optimal performance when the roller at the free end is pressed to 37 N. Extensive experiments were carried out on the final model of the winch, and position repeatability of under 50 mm deviation per 10 m was achieved through stable torque distribution under various payloads.

INDEX TERMS Rope winch, differential gear mechanism, position repeatability, capstan equation, rope tension modeling.

I. INTRODUCTION

As the number of high-rise buildings have increased in recent times, the demand for building maintenance has also increased. In order to extend the life of a building and increase its value, exterior wall maintenance tasks such as cleaning, inspecting, and painting are performed regularly. Most of the exterior building work are performed by workers who use a gondola or a rope fixed to the roof. Since most of the work is performed at great heights above the ground, workers are always at risk of falling. Therefore, many researchers have developed exterior building operating robots to ensure worker safety and improve work quality.

The associate editor coordinating the review of this manuscript and approving it for publication was Huiyu Zhou.

TITO 500 and Auto Façade Cleaning can ascend and descend in the vertical direction using a gantry fixed to the roof [1], [2]. This unmanned high-rise façade cleaning robot is modular and is mounted on the building's gondola to ascend/descend the building walls [3]. These robots use steel cables and can only be applied to buildings that have gantries. Therefore, the robots are not applicable to existing buildings, and additional gantry installations are required. To overcome these limitations and apply robots to existing buildings, robots with temporary installations have been developed. KITE and SkyScraper-I can be used by fixing a winch to an external frame or fixed obstacle [4], [5]. However, because steel cables have a large mass per unit volume and are very stiff, it is difficult to install a winch at the desired location along the exterior wall of a building.

A mobile-type robot has also been developed that minimizes the installation work on the exterior wall of the building; here, the winch is installed within the robot. The cable-driven parallel robot and the cleaning robot from Wall Robotics can ascend/descend using a winch inside the robot with cables connected to the roof of a building [6], [7]. However, if there is a climbing winch inside the robot, the weight of the steel cable is added to the payload, which has the disadvantage of consuming large amounts of power. IPC Eagle has a free end of ascending cable, so the payload applied to the winch does not change depending on the height of the robot [8]. However, for taller buildings, the weights of the steel cables are greater, rendering transportation and installation difficult. In addition, if the free end of the steel cable is shaken by disturbances such as wind, damages can be caused to the outer walls.

An appropriate winch mechanism that uses robots or machines can be selected for the automation of building maintenance work. At this time, the requirement of a gantry or installation location of the winch varies according to the environment in which the robot operates and the characteristics of the building. Seoul National University has developed a building cleaning robot that can be applied to general buildings without a gantry or winch mechanism for the robot [9], [10]. This winch mechanism is easy to install on the roof because it uses synthetic fiber rope that workers already use for exterior wall maintenance tasks. The winch structure has a free end so that temporary installation is possible, and the weight of the rope is not added to the payload.

One characteristic of the free-end-type winch is that it supports the weight of the structure using the frictional force between the winch and the cable or rope. Therefore, the payload is determined by the characteristics of the smaller among the actuator capacity of the winch and the friction between the winch and cable. According to the capstan equation, the friction between the winch and cable increases exponentially with the angle of the rope wound around the pulley [11]. In the case of insufficient friction, the rope slips and the winch falls, so it is important to maintain constant friction by maximizing the winding angle of the rope.

Various free-end-type winches have been developed for easy installation. ROPE RIDE uses a single pulley-type winch [9]. However, when only one pulley is used, the payload is low, and there are cases where the contact force is lost and the robot moves discontinuously during descent. Multiwound pulleys were used in capstan winch sailboats and powered rope ascenders to improve the ascending force [12], [13]. These mechanisms add a flange structure to prevent the ropes from slipping off, and can secure friction in proportion to the number of turns. However, there is a problem of low position accuracy and repeatability for climbing robots because sideways slippage cannot be prevented during motion.

A double-drum winch uses two grooved drums to prevent sideways slip [14]. The payload determines the rope tension of the load and the tension of the free end. The rope tension distribution around the pulley is determined by the values of these two tensions [15]. However, a short section of the rope provides the actual friction, and the remaining part does not affect the frictional force, which is inefficient in terms of power transmission. A cable traction control unit (CTCU) has been developed to detect the tension of the rope wound around multiple pulleys and to actively distribute the load [16]. However, tension must be detected in real-time for active control, and additional actuators are needed for load distribution.

This paper presents a free-end-type winch with high repeatability while maintaining the target payload. As mentioned above, the free-end-type winch can be easily applied to existing buildings because only the cable needs to be fixed to the roof of the building, and the weight of the cable is not added to the payload. However, since the position accuracy of the robot is reduced owing to slipping because the load is supported by the frictional force, the frictional force is secured through multiple windings. In the tension distribution, frictional forces are concentrated in certain parts of the rope, which is not only inefficient in terms of power but also adversely affects the durability of the rope.

Therefore, in this study, unlike other winches, a differential gear is applied to the winch to implement a structure that enables passive effective torque distribution. The differential structure distributes the torque automatically by adjusting the rotation amount of each pulley according to the force applied to each pulley when several pulleys are used. Torque distribution prevents unexpected slip of the rope by stably maintaining the torque applied to each pulley. In addition, torque loss due to friction can be minimized, thus enabling efficient actuator use. The winch proposed in this paper has design parameters that can be tuned, and the number and pressure of the pressure rollers can be adjusted to provide a specific number of windings of the rope and the frictional force.

In this paper, the number of windings of the rope is determined by a torque distribution analysis, and the design parameters are selected to maximize repeatability through experiments. Thus, two pulleys are connected in a differential structure, and the pressure roller has an optimal load distribution when pressed with a force of 37 N. In addition, in the above condition, position repeatability was found to be within 13 mm based on 2-sigma when moving 10-m lengths three times.

The remainder of this paper is organized as follows. Section 2 presents the kinematic structure and operating principle of the multiwound differential pulley winch (MWDPW). In section 3, an analysis of the rope tension distribution in the winch pulley with and without the differential structure is conducted and verified through experiments. Section 4 introduces experiments to determine the design parameters for optimizing MWDPW position repeatability. In section 5, a verification experiment is carried out in which torque distribution is effectively performed. The experiment demonstrates high repeatability performance in the final selected MWDPW. Conclusions are presented in Section 6.

II. STRUCTURE OF MULTIWOUND DIFFERENTIAL PULLEY WINCH (MWDPW)

Fig. 1 shows the overall structure of the proposed MWDPW. This winch weighs 20 kg and has dimensions of 600 mm (width), 600 mm (length), and 900 mm (height). The total payload is 220 N, and the climbing speed is 6 m/min. A traction pulley is wound by synthetic fiber rope to support the load through friction. In order to increase the friction, a greater rope length is wound around the traction pulley. To this end, three traction pulleys are used, where each pulley generates torque in proportion to the angle of the slip zone of the rope.

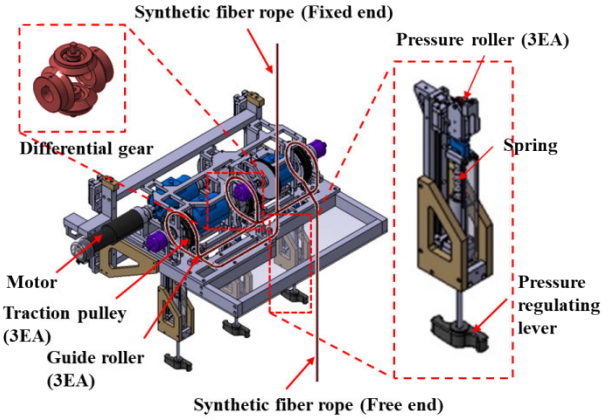

FIGURE 1. Structure of proposed multiwound differential pulley winch.

When multiple pulleys are synchronized and rotate at the same angle, the torque is concentrated on one pulley during ascent/descent, so the remaining pulleys cannot provide the frictional force. Ideally, slippage is minimized when equal force is applied to the traction pulley, and the loss of motor torque owing to friction is also minimized. Therefore, by adding a differential gear, a structure that passively distributes the torque between the pulley of fixed end and the pully of free end is designed. When the rope is wound around the traction pulley, it is equipped with a pressure roller to provide sufficient traction without slipping. The pressure roller can change the length of the spring by a lever that adjusts the pressure. As shown in Fig. 1, there is a section where the synthetic fiber rope is bent 90° between three pulleys, and a guide roller exists so that the rope does not leave the track.

The sensing system of the MWDPW is shown in Fig. 2. To measure the torque across each traction pulley, a torque sensor is connected to each pulley. Through this torque sensor, the torque distribution of the differential gear can be measured. The force applied to the pressure roller through the spring can be measured using a tension-and-compression-type load cell, and the amount of rotation of each pulley can be measured through the rotary encoder.

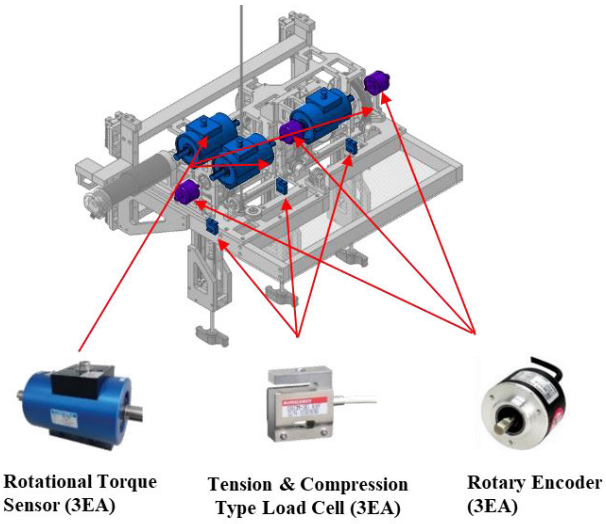

FIGURE 2. Schematic of sensor position in MWDPW.

III. MODELING OF TENSION DISTRIBUTION OF MWDPW

A. TENSION DISTRIBUTION OF A SINGLE PULLEY OF THE WINCH

The main feature of the tension distribution of the pulley is that the initial tension is amplified by the capstan equation. The capstan equation proposed by Euler is

$$T(\theta) = T_{initial} e^{\mu_k \theta} \tag{1}$$

where $T(\theta)$ is the rope tension at the position rotated by θ.

The traction force of the winch increases exponentially with the initial friction ($T_{initial}$) by the coefficient of kinetic friction (μ_k) and the winding angle (θ). The initial tension of the proposed winch is determined by the pressure roller. The relation between the compression force (P) of the pressure roller and the initial tension ($T_{initial}$) is

$$T_{initial} = \mu_{initial} P \tag{2}$$

where P is the compressive force, and $\mu_{initial}$ is the coefficient of kinetic friction with the initial tension caused by the compressive force applied perpendicular to the pulley surface. The actual initial tension adds not only frictional force to the pulley surface but also resistance due to the radial elasticity of the rope. However, in this study, only frictional force on the pulley surface is considered to simplify the model.

Substituting (2) in (1) and the angle wound on the pulley (θ_{wrap}) in θ, the maximum winch force ($T_{\max}$) can be obtained as follows:

$$T_{\max} = \mu_{initial} P e^{\mu_k \theta_{wrap}} \tag{3}$$

The initial friction coefficient and motion friction coefficient are determined by the shape and material of the mechanism. When the hardware is the same, the maximum climbing force ($T_{\max}$) is determined by the compression force and the winding angle. The maximum isometric force is proportional to the compressive force and increases exponentially with

respect to changes in the winding angle. Therefore, it is advantageous to increase the winding angle rather than the compressive force in order to increase the maximum climbing force. A conventional winch winds a rope several times in one friction cylinder [12], [13] or several pulleys in order to increase the winding angle [14], [16].

When the capstan equation is applied to a pulley, both slip and nonslip zones exist on the surface of the pulley. Slip zones are areas that slide on the pulley surface as the length of the rope decreases or increases owing to varying tension. On the other hand, the nonslip zone is an area where the tension does not change, and the rope length is constant so that the rope does not slip on the surface of the pulley. The rope speed in the slip zone can be obtained based on the rope speed in the nonslip zone [17]. According to Hooke's law, the deformation of the rope is proportional to tension, as follows:

$$\varepsilon(\theta) = \frac{T(\theta)}{AE} \tag{4}$$

where A is the cross section of the rope, and E is its Young modulus. In this work, it is assumed that the change in the cross-sectional area is relatively small, and the value is regarded as a constant. The angular velocity of the rope element in the slip zone is determined by the amount of strain when the rope is stretched or compressed, and the amount of strain is proportional to the tension, as shown in (4). Therefore, the following equation can be obtained:

$$v(\theta) = v_{ref}(1 + \varepsilon(\theta)) = v_{ref}\left(1 + \frac{T(\theta)}{AE}\right) \tag{5}$$

where v_{ref} is the rope element speed in the nonslip zone. According to (5), the speed of the rope is proportional to the change in rope tension. As θ increases, the tension changes exponentially according to the capstan equation, and the speed of the rope changes exponentially.

The tension distribution of the rope on one pulley changes the position of the slip and nonslip zones according to the direction of rotation of the pulley, as shown in Fig. 3 [17], [18]. M is the torque transmitted to the pulley by the drive motor, and ω is the angular velocity of the pulley.

As the winch ascends, the pulley winds up the rope with higher loading tension, so the pulley rotates from the region of higher rope tension to lower rope tension. The rotation direction of the pulley is the same as the rotation direction of the motor torque. The slip zone and the nonslip zone when rising are shown in Fig. 3(a). When the winch is descending, the pulley rotates from the region of low rope tension to high rope tension, and the motor torque and pulley rotate in different directions. In this case, the slip and nonslip zones are as shown in Fig. 3(b).

The larger the winding angle, the greater is the climbing force. However, the speed difference between the rope and the pulley exponentially increases, causing damage to the rope and the pulley by friction. Thus, for durability, a mechanism is needed to allow the pulley to move at different speeds.

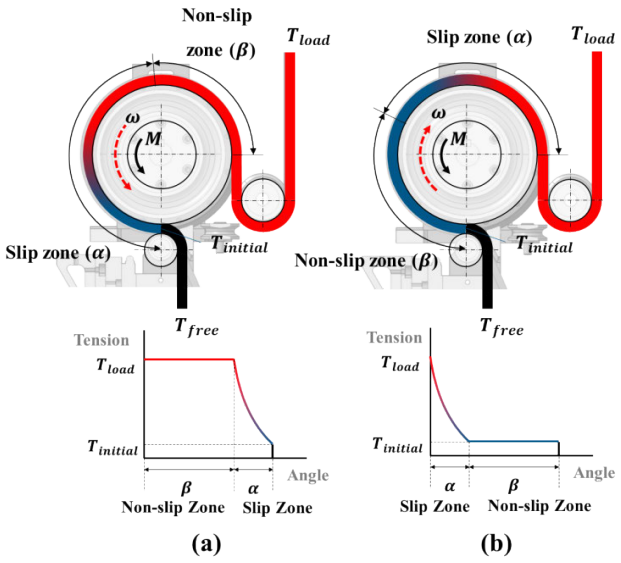

FIGURE 3. Tension distribution graph in (a) ascending motion and (b) descending motion.

B. TENSION DISTRIBUTION ANALYSIS OF MULTIPLE PULLEYS OF THE WINCH

A conventional winch is designed to wind the rope several times to increase the maximum ascending power. The proposed multiwound differential pulley winch is designed not only to increase the maximum ascending force but also to distribute the same traction force to multiple pulleys to minimize damage to the ropes and pulleys. The traction force on each pulley is distributed passively with the differential mechanism built into the winch (as introduced in Section 2). Herein, based on the capstan equation, the tension distribution of the rope in the winch depends on the existence of the differential mechanism and how it affects the traction force. The validity of the derived equation is demonstrated by experiments in Section 3.3. There are four cases of the winch to derive the tension distribution, as shown in Fig. 4. In all cases, it is assumed that the pressure rollers are pressed with the same compression force while pressing the same position of the traction pulley.

1) RIGID SHAFT AND TRIPLE WINDING ROPE CASE (CASE 1)

If the rope is wound around several pulleys rotating at the same speeds, it can be assumed to be the same as if wound several times on one cylinder. As discussed in Section 3.1, slip and nonslip zones exist in different positions depending on the direction of rotation. Therefore, when ascending or descending, the position of the slip zone moves in the transient phase. If the payload applied to the winch can afford enough of the ascending force generated by one of the pulleys, then the slip zone exists only in one pulley. For example, if three pulleys are rotated at the same time as in case 1, a slip zone is created in pulley 3 when it ascends, and a slip zone is located in pulley 1 when descending.

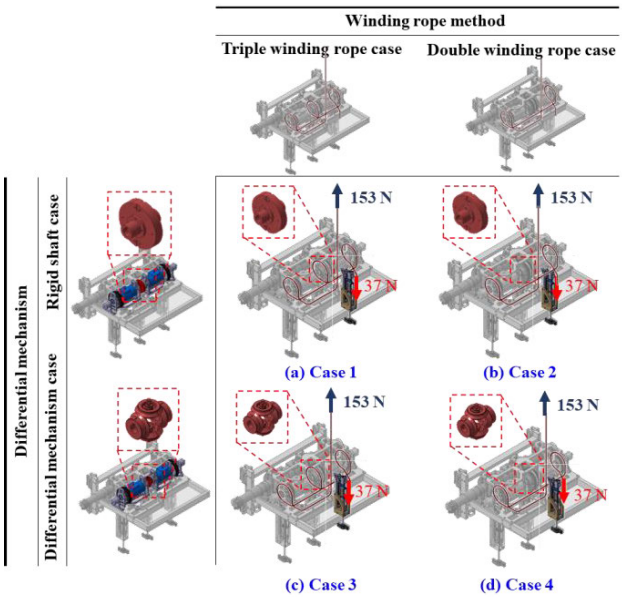

FIGURE 4. Verification cases of tension distribution analysis of multiple pulleys of winch.

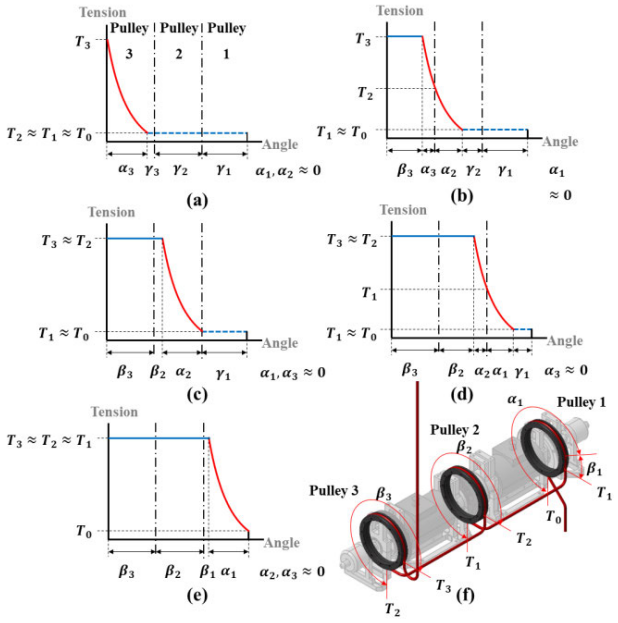

FIGURE 5. Tension distribution of triple pulleys connected by rigid shaft when switching from descending to ascending motion (a) Tension distribution during descending motion (start of change of direction of movement) (b)–(d) Tension distribution shift when switching from descending to ascending motion (e) Tension distribution during ascending motion (end of change of direction of movement) (f) Notations of slip zone and nonslip zones and tensions on triple pulleys.

When descending using a winch with three pulleys and then changing direction, the expected tension distribution graph is as shown in Fig. 5. α represents an effective slip zone that generates traction forces, and β represents a nonslip zone with no slip and no change in tension. γ is theoretically a nonslip zone, but this is an ineffective slip zone where slip exists continually owing to the difference in the rope speed and pulley angular velocity. In region γ, the tensile strength is very low, so little traction force is generated.

In the general case where the pulley rotates in only one direction, there is no change of tension in the nonslip zone, as shown in Fig. 3(a) and Fig. 3(b). The nonslip zone is β, represented by a flat solid line in Fig. 5(b)–(d). In the β region, no traction force is generated. Finally, the γ zone shows little change in tension and is represented by a dotted line. The γ zone is a section in which the tension is constant and the speed is maintained but it is continuously slipping. There is a speed difference before and after the slip zone, and the nonslip zone causes the rope to wind at a constant speed. However, if all pulleys are rotating at the same speed, then the rope speed before and after the slip zone cannot be the same. In this case, the rope exits on the surface of the pulley. Because this slip has a small frictional force, there is no change in tension, and it generates very little traction force.

Fig. 5. (b)–(d) show that the slip zone moves sequentially from pulley 3 to pulley 1 through pulley 2. A slip zone is a section where frictional force is generated and which generates the actual traction force. Fig. 5(b) shows that because the slip zones are in pulley 3 and pulley 2, the traction force is also distributed in pulley 3 and pulley 2, and ineffective slip zones that do not generate traction force also exist in pulley 2 and pulley 1. Fig. 5(c) is a case in which the slip zone is only in pulley 2. In this case, pulley 3 and pulley 1 do not produce traction forces because there is no change in tension. In case 5(d), as in case 5(b), the slip zone exists across two pulleys. After enough time, pulley 1 generates traction force, as shown in Fig. 5(e).

When changing the direction of ascent and descent using three pulleys, the tension distribution is opposite to the situation of Fig. 5, and the results are shown in Fig. 6. The slip zone then moves from pulley 1 to pulley 3. The descending case is different from the ascending case in the ineffective slip zone.

Since the speed of the winch is determined based on where the rope enters, the nonslip zone is located in pulley 1 with low tension, and pulley 3 has an ineffective slip zone. Because of the low tension in the nonslip zone, the ropes around pulley 1 and pulley 2 are weakly bonded to the pulley, which can lead to a stick-slip phenomena.

Therefore, the winch is designed to increase the value of T_0 by adding a pressure roller to a mechanism that can have high repeatability even when descending. The optimum parameters for the pressure roller were derived from the experiment in Section 4.

2) RIGID SHAFT AND DOUBLE WINDING ROPE CASE (CASE 2)

The tension distribution when ascending and descending using two pulleys with the same rotation speed is shown in Fig. 7 and Fig. 8. This works on the same principle as when there are three pulleys.

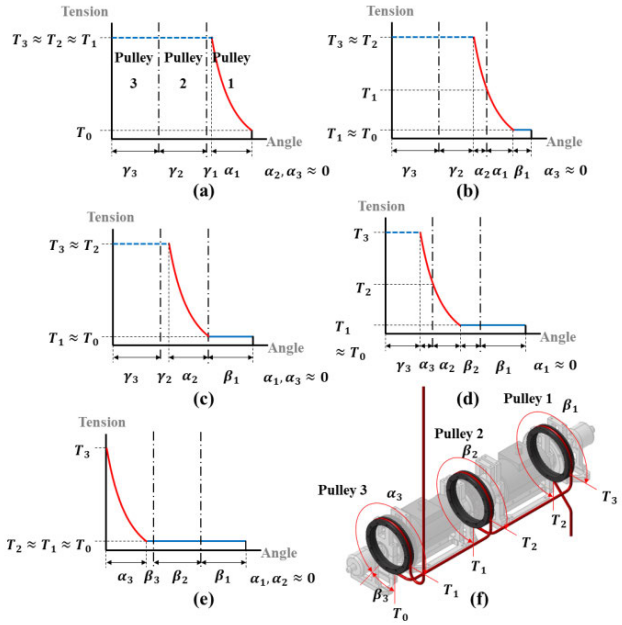

FIGURE 6. Tension distribution of triple pulleys connected by rigid shaft when switching from ascending to descending motion (a) Tension distribution during ascending motion (start of change of direction of movement) (b)–(d) Tension distribution shift when switching from ascending to descending motion (e) Tension distribution during descending motion (end of change of direction of movement) (f) Notations of slip zone and nonslip zones and tensions on triple pulleys.

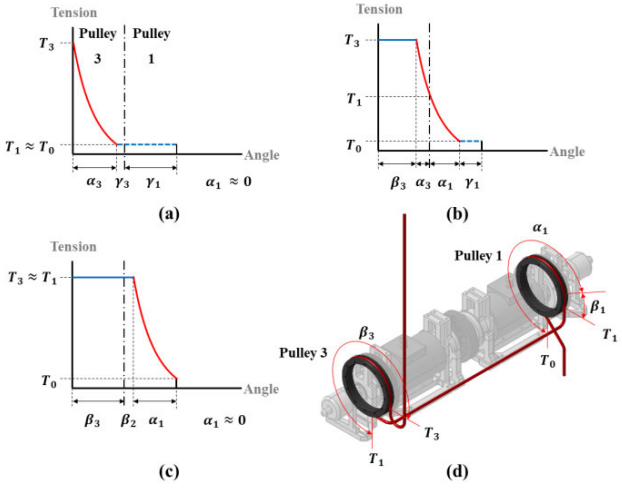

FIGURE 7. Tension distribution of double pulleys connected by rigid shaft when switching from descending to ascending motion (a) Tension distribution during descending motion (start of change of direction of movement) (b) Tension distribution shift when switching from descending to ascending motion (c) Tension distribution during ascending motion (end of change of direction of movement) (d) Notations of slip zone and nonslip zones and tensions on double pulleys.

3) DIFFERENTIAL MECHANISM AND TRIPLE WINDING ROPE CASE (CASE 3)

In the previous section, the distribution of rope tension was explained when the multipulley rotates at a synchronized speed. This winch mechanism has disadvantages in terms of

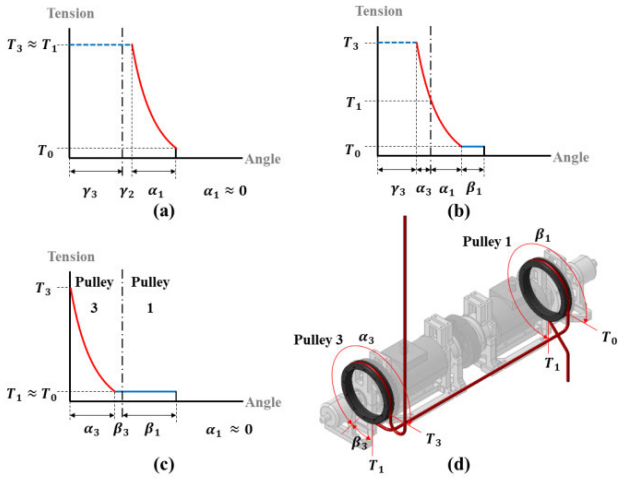

FIGURE 8. Tension distribution of double pulleys connected by rigid shaft when switching from ascending to descending motion (a) Tension distribution during ascending motion (start of change of direction of movement) (b) Tension distribution shift when switching from ascending to descending motion (c) Tension distribution during descending motion (end of change of direction of movement) (d) Notations of slip zone and nonslip zones and tensions on double pulleys.

performance and durability because only one pulley holds a traction force in most cases. Therefore, the MWDPW proposed in this paper aims to increase the durability of the winch and positioning performance via eliminating ineffective slip zones by uniformly distributing the torque applied to each pulley using a differential mechanism. Here, tension distribution through the differential gear mechanism is derived analytically.

The differential mechanism maintains the torques of pulley 1 and pulley 3 at constant rates, and retains the difference between the angular velocities of pulley 1 and pulley 2 and the angular velocities of pulley 2 and pulley 3. Slip zones exist on all pulleys because different pulleys can rotate at different speeds. Based on previous studies on the tension distribution of ropes connected to pulleys with different velocities, it is assumed that there are two slip zones in pulley 2 [11], [15], [19].

First, when three pulleys are connected by a differential gear, as shown in case 3 in Fig. 4(c), the tension distribution of each pulley can be derived by the capstan equation and the torque distribution equation of the differential gears as follows. The slip zone of each pulley is α, and the nonslip zone is β. The tension and rope speed on each pulley are shown in Fig. 9. Fig. 9(a) shows the rotation speed of each pulley when ascending. Fig. 9(b), (c), and (d) represent parameters related to the speeds of pulley 3, pulley 2, and pulley 1, respectively. The rotation speed of each pulley can be derived as follows.

First, pulley 2 rotates synchronously with the motor. Based on pulley 2, the differential gear mechanism is operated by the torque difference between pulley 1 and pulley 3. The rope rotation speed of the nonslip zone on pulley 2 is the same

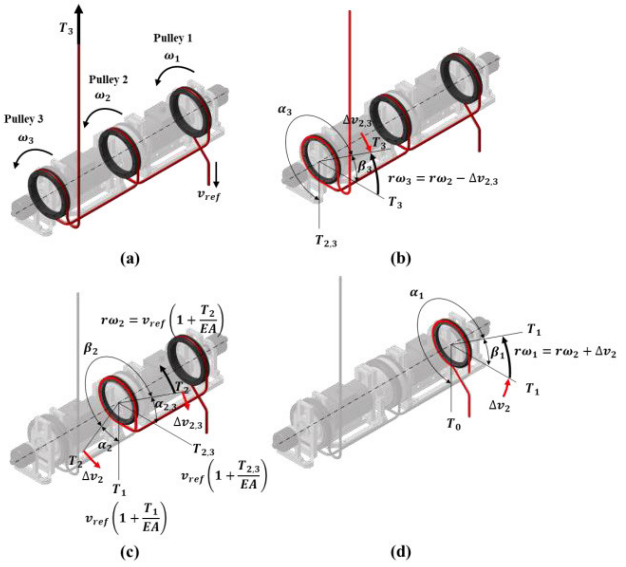

FIGURE 9. Notation of velocity and tension of (a) entire winch, (b) pulley 3, (c) pulley 2, and (d) pulley 1 during ascending motion with differential mechanism and triple pulleys.

as the motor speed. Two slip zones, α_2 and $\alpha_{2,3}$, are located before and after the nonslip zone. The velocity in each slip zone is related to the magnitude of the rope tension and can be expressed by the capstan equation as follows:

$$r\omega_2 = v_{ref}\left(1 + \frac{T_2}{EA}\right) \tag{6}$$

The angular velocities of pulleys 1 and 3 can be obtained by adding the speed change of the slip zone owing to the tension difference to the angular velocity of pulley 2 according to the rotational direction.

$$\begin{cases} r\omega_1 = r\omega_2 + \Delta v_2 \\ r\omega_3 = r\omega_2 - \Delta v_{2,3} \end{cases} \tag{7}$$

where

$$\begin{cases} \Delta v_2 = v_{ref}\left(1 + \dfrac{T_2}{EA}\right) - v_{ref}\left(1 + \dfrac{T_1}{EA}\right) \\ \Delta v_{2,3} = v_{ref}\left(1 + \dfrac{T_3}{EA}\right) - v_{ref}\left(1 + \dfrac{T_2}{EA}\right) \end{cases}$$

From (7), the speeds of pulleys 1 and 3 can be expressed as an expression of rope tension in the nonslip zone of each pulley.

$$\begin{cases} r\omega_1 = v_{ref}\left(1 + \dfrac{2T_2 - T_3}{EA}\right) \\ r\omega_1 = v_{ref}\left(1 + \dfrac{2T_2 - T_1}{EA}\right) \end{cases} \tag{8}$$

According to the principle of the differential mechanism, the angular velocity of pulley 2 is equal to the average of the angular velocities of pulleys 1 and 3.

$$\omega_1 + \omega_3 = 2\omega_2 \tag{9}$$

Substituting (6) and (8) into (9) gives the following equation for rope tension:

$$T_3 - T_2 = T_2 - T_1 \tag{10}$$

The torque applied to pulley 1 and pulley 3 is equally distributed by the differential gear mechanism. When the torque applied to each pulley is τ_1, τ_2, and τ_3, the following relation is established:

$$\tau_1 = \tau_3 \tag{11}$$

(10) and (11) are two relation equations in ascending motion added by the differential gear mechanism. The torque applied to the pulley is equal to the rope tension difference in the slip zone of the pulley. Therefore, the tension distribution in the pulleys of the winch with the differential gear mechanism is obtained as shown in Fig. 10.

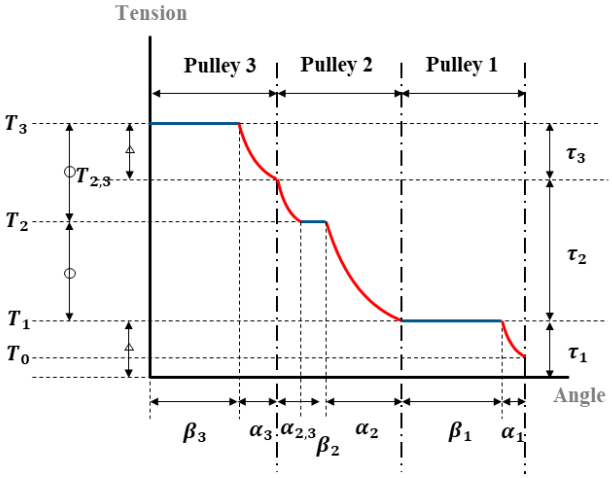

FIGURE 10. Tension distribution of triple pulleys connected by differential mechanism during ascending motion.

The tension distribution for descending using a given winch mechanism is also derived. The parameters related to the speed of each pulley when descending are shown in Fig. 11.

In a descending motion, the speeds of pulley 1 and pulley 3 are derived based on the angular velocity of pulley 2. The rotation speeds of pulleys 1 and 3 can be obtained by adding the speed change of the slip zone owing to the tension difference to the angular velocity of pulley 2 according to the direction of rotation.

$$\begin{cases} r\omega_1 = r\omega_2 - \Delta v_2 \\ r\omega_3 = r\omega_2 + \Delta v_{2,3} \end{cases} \tag{12}$$

where

$$\begin{cases} \Delta v_2 = v_{ref}\left(1 + \dfrac{T_2}{EA}\right) - v_{ref}\left(1 + \dfrac{T_0}{EA}\right) \\ \Delta v_{2,3} = v_{ref}\left(1 + \dfrac{T_{2,3}}{EA}\right) - v_{ref}\left(1 + \dfrac{T_2}{EA}\right) \end{cases}$$

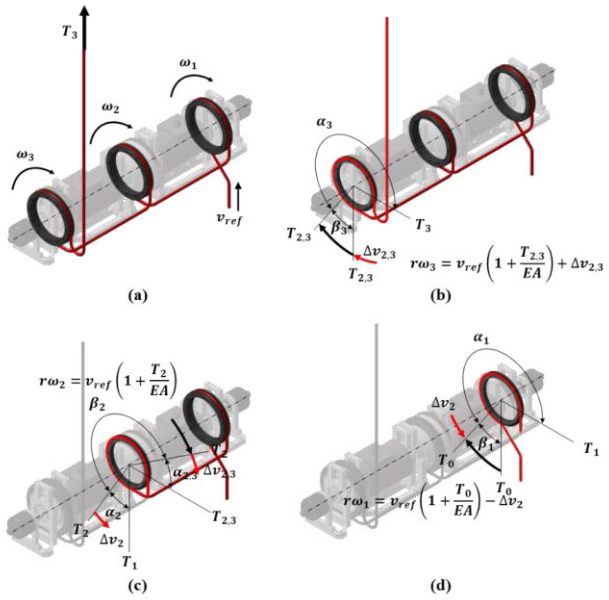

FIGURE 11. Notation of velocity and tension of (a) entire winch, (b) pulley 3, (c) pulley 2, and (d) pulley 1 during descending motion with differential mechanism and triple pulleys.

Substituting (6) and (12) into (9) gives the following equation for the rope tension:

$$T_{2,3} - T_2 = T_2 - T_0 \tag{13}$$

Equations (13) and (11) are relation equations with regard to the descending motion added by the differential gear mechanism. Thus, when a winch with a differential gear mechanism descends, the distribution of tension in the pulleys has the shape shown in Fig. 12.

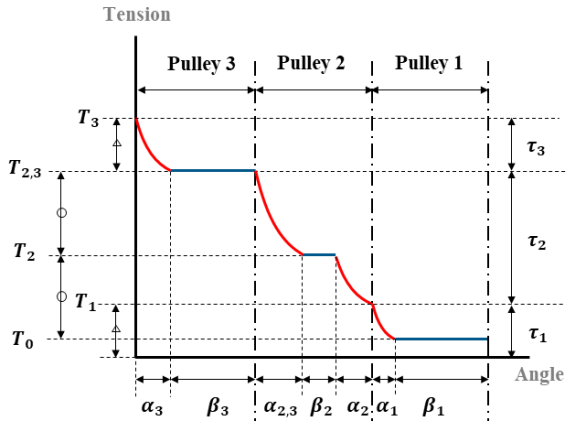

FIGURE 12. Tension distribution of triple pulleys connected by differential mechanism during descending motion.

Ideally, by connecting three pulleys through a differential mechanism, the performance of the winch can be improved by equally distributing the torque across each pulley. However, there are some cases of satisfying two relations, and there may be extreme cases where torque is not applied to pulley 2, as shown in Fig. 13. This is the case when T_1 is larger than T_2 and the tension is increased in the slip zone at pulley 2. These results show that using many pulleys is not always advantageous for torque distribution.

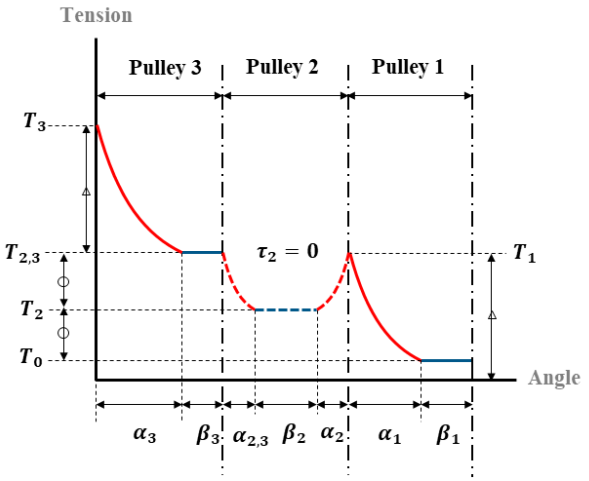

FIGURE 13. Example of tension distribution of triple pulleys connected by differential mechanism during descending motion.

4) DIFFERENTIAL MECHANISM AND DOUBLE WINDING ROPE CASE (CASE 4)

The differential mechanism and double winding rope case is analyzed in this section with regard to the tension distribution. As in the triple winding rope case, the relation can be found by combining the capstan equation and the differential mechanism equation. The tension distribution during an ascending motion is derived. The parameters related to the speed of each pulley when ascending are shown in Fig. 14.

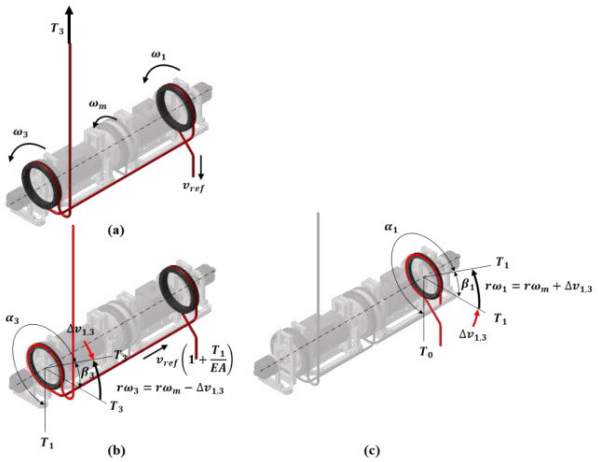

FIGURE 14. Notation of velocity and tension of (a) entire winch, (b) pulley 3, and (c) pulley 1 during ascending motion with differential mechanism and double pulleys.

When the speed of the differential gear connected to the motor is, ω_3 the speeds of pulleys 1 and 3 can be obtained by

adding the speed change of the slip zone owing to the tension difference.

$$\begin{cases} r\omega_1 = r\omega_m + \Delta v_{1,3} \\ r\omega_3 = r\omega_m - \Delta v_{1,3} \end{cases} \tag{14}$$

where

$$\begin{cases} r\omega_m = v_{ref}\left(1 + \dfrac{T_1}{EA}\right) \\ \Delta v_{1,3} = v_{ref}\left(1 + \dfrac{T_3}{EA}\right) - v_{ref}\left(1 + \dfrac{T_1}{EA}\right) \end{cases}$$

Through (14), the speeds of pulleys 1 and 3 can be expressed as the rope tension in the nonslip zone of each pulley.

$$\begin{cases} r\omega_1 = v_{ref}\left(1 + \dfrac{2T_1}{EA}\right) \\ r\omega_3 = v_{ref} \end{cases} \tag{15}$$

According to the principle of the differential mechanism, the angular velocity of pulley 2 is equal to the average of the angular velocities of pulleys 1 and 3, as shown in (9).

Substituting (14) and (15) into (9) gives the following equation for the rope tension:

$$T_3 = 2T_1 \tag{16}$$

The torques applied to pulley 1 and pulley 3 are equally distributed by the differential gear mechanism, so if the torque applied to each pulley is τ_1 and τ_3, respectively, then (11) holds. Therefore, when descending using the winch of a double winding rope with a differential gear mechanism, the tension distribution of the pulleys has the shape shown in Fig. 15.

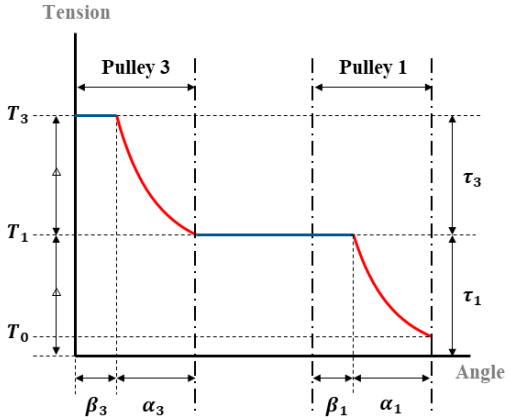

FIGURE 15. Tension distribution of double pulleys connected by differential mechanism during ascending motion.

The parameters related to the speed of each pulley when descending are shown in Fig. 16. In a descending motion, the speeds of pulley 1 and pulley 3 can be derived as follows:

$$\begin{cases} r\omega_1 = r\omega_m - \Delta v_{0,1} \\ r\omega_3 = r\omega_m + \Delta v_{0,1} \end{cases} \tag{17}$$

where

$$\begin{cases} r\omega_m = v_{ref}\left(1 + \dfrac{T_1}{EA}\right) \\ \Delta v_{0,1} = v_{ref}\left(1 + \dfrac{T_1}{EA}\right) - v_{ref}\left(1 + \dfrac{T_0}{EA}\right) \end{cases}$$

By substituting (17) into (9) of the differential gear mechanism, (16) and (11) can be derived. Therefore, when ascending using the winch of a double winding rope with a differential gear mechanism, the tension distribution of the pulleys has the shape shown in Fig. 17.

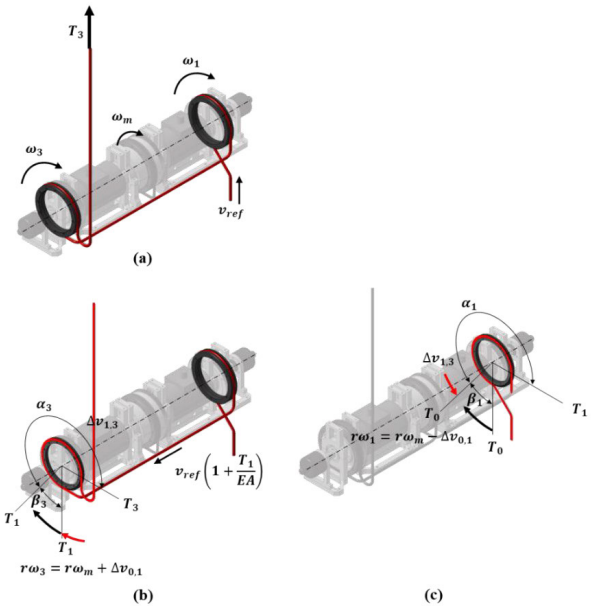

FIGURE 16. Notation of velocity and tension of (a) entire winch, (b) pulley 3, and (c) pulley 1 during descending motion with differential mechanism and double pulleys.

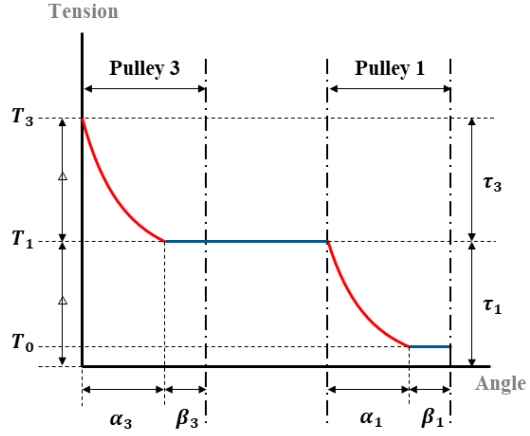

FIGURE 17. Tension distribution of double pulleys connected by differential mechanism during descending motion.

C. EXPERIMENT FOR TENSION DISTRIBUTION ANALYSIS

1) TEST BENCH FOR MODEL VERIFICATION OF PULLEY TENSION DISTRIBUTION

A test bench is shown in Fig.18 and used to verify the model of the tension distribution. The height of the test bench is

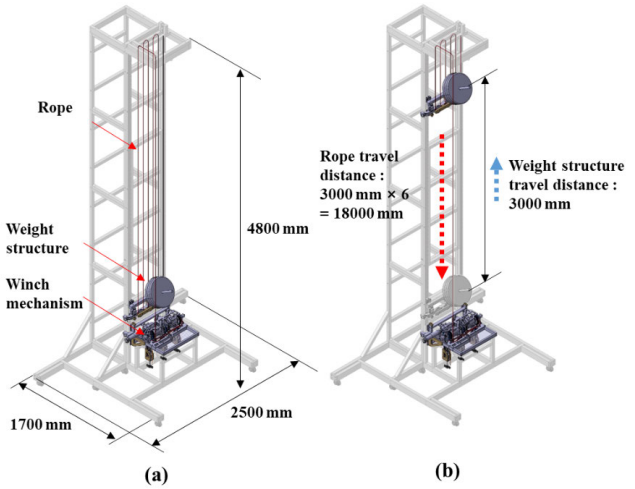

FIGURE 18. (a) Test bench dimensions and components when weight structure is at bottom-limit position, (b) weight structure at upper-limit position.

4800 mm, and the test area of the winch is 3000 mm. Movable pulleys are added for testing in the same environment as in actual building applications, and the total rope travel distance is 18,000 mm. To verify the performance of this winch at various payloads, a weight structure is added to the winch mechanism. If the load weight of the winch is different, then the tension of the rope of the loading part is also different, so the torque distribution over the entire pulley changes. The proposed winch mechanism is expected to achieve stable ascending/descending performance for various payloads because torque distribution is possible through the differential mechanism.

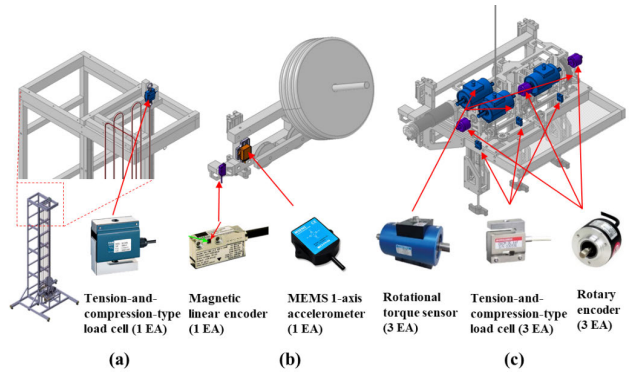

FIGURE 19. Sensors on (a) test bench, (b) weight structure, and (c) winch mechanism.

The sensor used to evaluate the performance of the winch mechanism is shown in Fig. 19. The rope tension is measured by a load cell mounted on the top of the test bench, as shown in Fig. 19(a). The actual position is measured by a magnetic linear encoder attached to the weight structure. Acceleration of the weight structure is also measured by the MEMS one-axis accelerometer, as shown in Fig. 19(b). There are three torque sensors between the traction pulleys and driving motor. The actual traction force generated by the traction pulleys can be measured in real time with these torque sensors. Three load cells at the rollers measure the pressure of the rollers. Three rotary sensors measuring the rotation degree of each traction pulley indicate activation of the differential mechanism. These sensors are located on the winch mechanism, as shown in Fig. 19(c).

2) RIGID SHAFT AND TRIPLE WINDING ROPE CASE (CASE 1)

An experiment is conducted to verify the tension distribution for three pulleys connected to a rigid shaft and rotating at the same speed. During an ascending motion, the slip zone moves from pulley 3 to pulley 1 as shown in Fig. 5, and pulley 1 carries all of the payload in the final state. During a descending motion, the slip zone moves from pulley 1 to pulley 3 as shown in Fig. 6, and pulley 3 carries all payload in the final state. In order to verify the tension distribution model, the experiment is performed for ascending and descending 10 m for 80 s on the test bench, and the results are shown in Fig. 20(a).

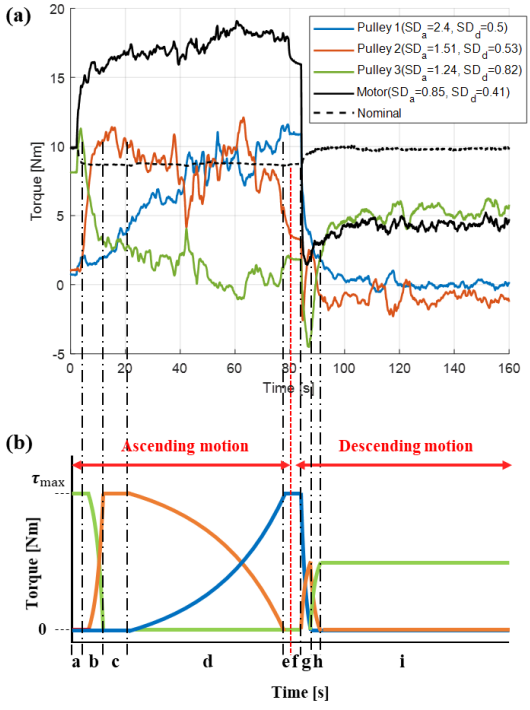

FIGURE 20. (a) Experimental results and (b) prediction results based on tension distribution analysis of rigid shaft and triple winding rope case.

Fig. 20(b) is a torque prediction graph in the time domain based on the torque distribution model of pulleys a, b, c, d, and e in the time domain of Fig. 20(b). This corresponds to cases a, b, c, d, and e in Fig. 5. Cases f, g, h, and i in Fig. 20(b) correspond to the cases of a, b, d, and e in Fig. 6. This confirms that the torque distribution is moving in the expected manner, and the payload is concentrated on one pulley in the final state. The main cause of the prediction error is the frictional force between the rope and the pulley.

However, this is not included in the model owing to the presence of an ineffective slip zone.

In addition, owing to the nonlinearly extending characteristic of the flexible rope and the wedge shape of the pulley surface, noise is included in the tension component. When moving at the same speed under the same payload, the winch has a constant motor torque. However, as shown in Fig. 20, frictional losses occur. In conclusion, as expected from Section 3.2.1, when three pulleys are rotated at the same speed, the load is concentrated in one pulley, which adversely affects the durability. In addition, it can be considered that the power efficiency of the motor owing to friction loss is also reduced.

3) RIGID SHAFT AND DOUBLE WINDING ROPE CASE (CASE 2)

An experiment is conducted to verify the tension distribution when two pulleys are connected by a rigid shaft and rotated at the same speed. The experimental conditions are the same as those in Section 3.2.1, and the experimental results are shown in Fig. 21.

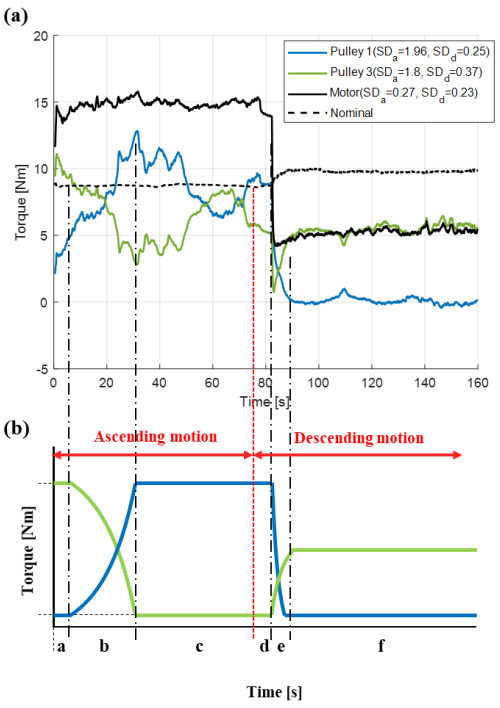

FIGURE 21. (a) Experimental results and (b) prediction results based on tension distribution analysis of rigid shaft and double winding rope case.

In the case of two pulleys, the overall graph of the tension distribution is similar to that of three pulleys. During an ascending motion, the slip zone moves the pulley as shown in Fig. 7, and all of the payload is applied to pulley 1 in the final state. During a descending motion, the slip zone moves from pulley 1 to pulley 3 as shown in Fig. 8. After a sufficient time, pulley 3 takes all of the payload. The experimental results are shown in Fig. 21(b). The experiment confirmed that the torque concentrates on one pulley. Thus, when using pulleys connected by rigid shafts, if the payload is constant, then there is little difference from using only one pulley in terms of durability.

4) DIFFERENTIAL MECHANISM AND TRIPLE WINDING ROPE CASE (CASE 3)

An experiment is performed to verify the torque distribution model for the winch using a differential mechanism. The experiment is carried out for a situation in which three pulleys are connected. In this case, as derived in Section 3.2.3, the torques of pulley 1 and pulley 3 are the same, and this confirms that (10) holds for the rope tension applied to the nonslip zone of each pulley. The results of the ascending and descending tests on the test bench are shown in Fig. 22.

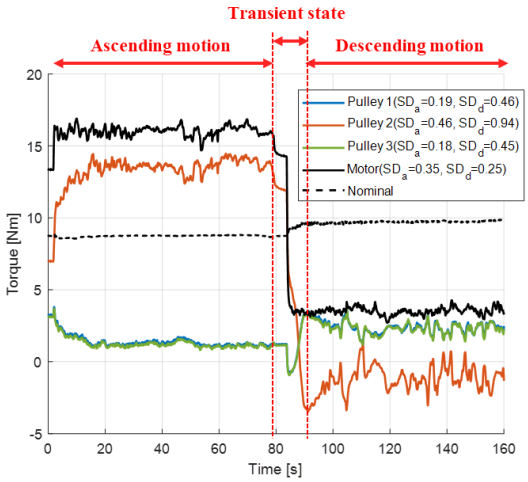

FIGURE 22. Experimental results of differential mechanism and triple winding rope case.

As assumed in the torque distribution model, the torque values of pulleys 1 and 3 are measured to be identical, and the tension distribution does not change during the descent. The payload is concentrated on pulley 2 when ascending, and the payload is distributed on pulleys 1 and 3 when descending. The result of analyzing the tension distribution is shown in Fig. 23.

As shown in Fig. 23(a), if the slip zone is distributed at large angles on both sides of pulley 2, then the maximum torque can be concentrated on pulley 2. At the same time, pulley 1 and pulley 3 have low traction forces, as shown in Fig. 22, because the slip zone is very short. During a descending motion, rope tension is not applied to pulley 2, but torque is distributed only to pulley 1 and pulley 3. It can be seen that this corresponds to the situation in Fig. 23(b). As shown above, when three pulleys are connected by the differential gear mechanism, the torque of pulley 2 cannot be calculated accurately by (10) and (11), which limits the position predictions. In addition, tension can be concentrated in one or two pulleys, but this does not meet the development purpose of applying equal torque to all pulleys.

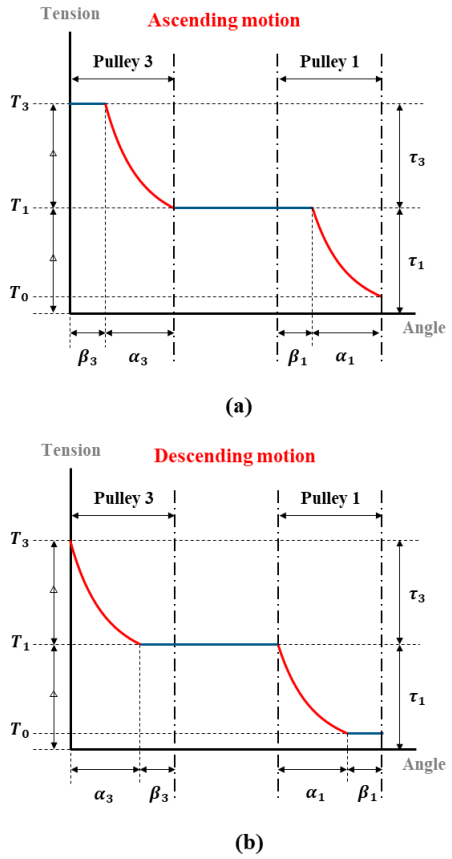

FIGURE 23. Tension distribution of triple pulleys connected by differential mechanism during (a) ascending and (b) descending motion.

5) DIFFERENTIAL MECHANISM AND DOUBLE WINDING ROPE CASE (CASE 4)

The results of the ascending and descending experiments for the winch connecting two pulleys with a differential mechanism are as follows.

As expected from the equation derived in Section 3.2.4, the torques of pulley 1 and pulley 3 are distributed equally through the differential mechanism when ascending and descending. The torque distributions at this time are shown in Fig. 15 and Fig. 17, respectively. Therefore, Case 4 can be considered as the best case in terms of torque distribution and durability. The differences between the maximum and minimum values and standard deviation values for the torque of each pulley for all four cases are listed in Table 1 and 2.

TABLE 1. Max-min values of pulley torques.

Motion	Case 1	Case 2	Case 3	Case 4
Ascending [Nm]	13.17	10.05	13.66	0.94
Descending [Nm]	8.34	6.90	7.25	0.70

As shown in Tables 1 and 2, Case 4 shows the smallest difference between the maximum and minimum values and torques, and the smallest standard deviation of the pulley when ascending and descending. Therefore, this MWDPW adopts the final mechanism to connect two pulleys using a differential mechanism.

A constant torque distribution means that the effect of the ineffective slip zone is small, so the positioning repeatability can be expected to be low. In Section 4, the position repeatability will be optimized.

TABLE 2. Standard deviation of traction pulley torques.

Motion	Subject	Case 1	Case 2	Case 3	Case 4
Ascending	Pulley 1 [Nm]	2.40	1.96	0.19	0.13
	Pulley 2 [Nm]	1.51	-	0.46	-
	Pulley 3 [Nm]	1.24	1.80	0.18	0.14
	Motor [Nm]	0.85	0.27	0.35	0.24
Descending	Pulley 1 [Nm]	0.50	0.25	0.46	0.11
	Pulley 2 [Nm]	0.53	-	0.94	-
	Pulley 3 [Nm]	0.82	0.37	0.45	0.12
	Motor [Nm]	0.41	0.23	0.25	0.22

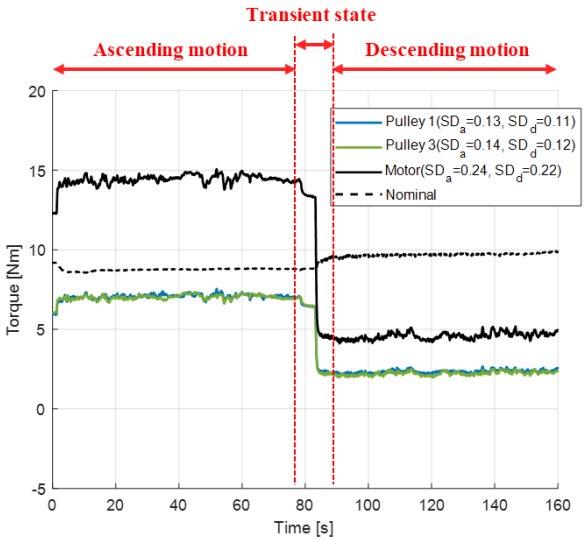

FIGURE 24. Experimental results of differential mechanism and double winding rope case.

IV. OPTIMIZATION OF DESIGN PARAMETER FOR HIGHLY REPEATABLE MWDPW

In the previous section, the torque distribution performance of the proposed winch mechanism proved optimal when two pulleys were connected to the differential gear. The position repeatability criteria are first defined to evaluate the performance of a given winch mechanism. In addition, various experiments are conducted to maximize the performance of a winch based on position repeatability. Based on this, the design parameters of the MWDPW are optimized.

A. REPEATABILITY CRITERION

The winch performance is measured according to the ISO regulation for the determination of position accuracy and

repeatability of numerically controlled axes [20]. Accuracy and repeatability are calculated by repeatedly measuring the actual moving position of several target positions. The standard measuring cycle is shown in Fig. 25(a). The revised measuring cycle is used because the winch mechanism continues to deviate from its initial position. The initial position is initialized as shown in Fig. 25(b) for each cycle.

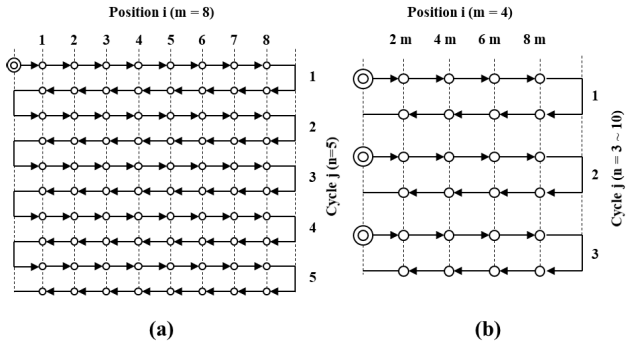

FIGURE 25. (a) Standard measuring cycle and (b) revised measuring cycle for winch.

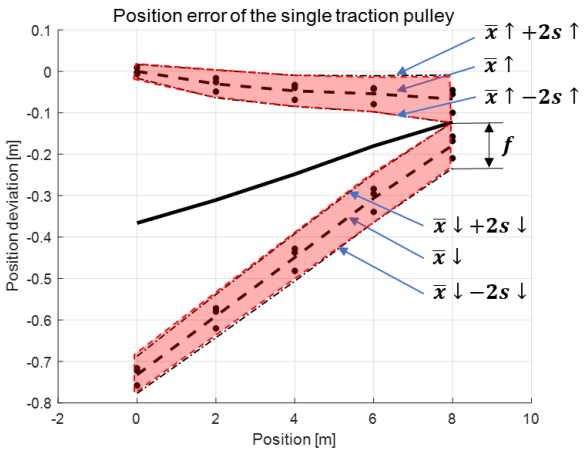

FIGURE 26. Accuracy and repeatability graph and $\pm 2s$ range.

The accuracy and repeatability graph is shown in Fig. 26. The position deviation x at each target position is calculated as follows:

$$x_{ij} = P_{ij} - P_i \tag{18}$$

where P_i is target position and P_{ij} is actual position.

Mean unidirectional positioning deviations ($\overline{x_l}\uparrow, \overline{x_l}\downarrow$) are mean values according to the direction. The unidirectional axis positioning repeatability ($s_i\uparrow, s_i\downarrow$) are the same as those for the sample standard deviation, as follows:

$$s_i\uparrow = \sqrt{\frac{1}{n-1}\sum_{j=1}^{n}(x_{ij}\uparrow - \bar{x}_l)^2} \tag{19}$$

$$s_i\downarrow = \sqrt{\frac{1}{n-1}\sum_{j=1}^{n}(x_{ij}\downarrow - \bar{x}_l)^2} \tag{20}$$

The graph in Fig. 25 shows the $\pm 2s$ range of the mean value. If the data are normally distributed, this means that 95% of the data may be in that area. A small $\pm 2s$ means that the same results can be obtained under the same conditions. It is important to have high repeatability in order to reduce the position prediction errors. This is because predictions based on physical models will always show the same results under the same conditions.

The position repeatability performance of the MWDPW is evaluated on the test bench, and the results are shown in Fig. 18. This test bench adds a weight structure to the winch mechanism to test the performance of the winch at various payloads. If the payload changes, then the tension of the loading part also changes, so the torque distribution across the pulley also changes. However, the proposed winch mechanism is expected to achieve high position repeatability for various payloads because the ineffective slip zone can be minimized through the differential mechanism. The experiment is performed by measuring the position of the winch as it ascends and descends. This is shown in Fig. 27 according to the criteria defined in Fig. 25(b).

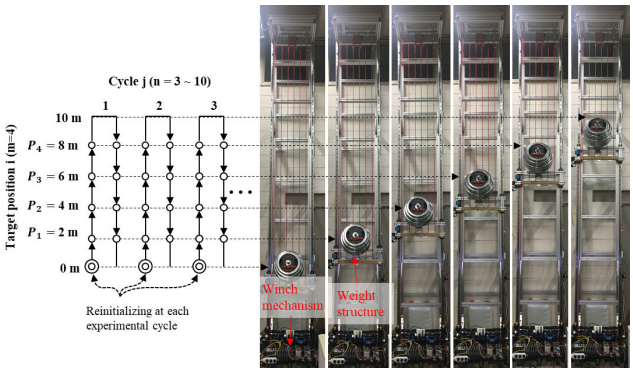

FIGURE 27. Test bench for position repeatability measurement.

B. OPTIMIZATION OF OPERATING CONDITIONS FOR MWDPW

The function of a pressure roller is to increase the normal force between the rope and the surface of the traction pulley so that the initial tension is produced by the friction. There must be an initial tension because additional tension depends on the initial tension. From the capstan equation, the final tension is multiplied by the initial tension.

In order to optimize the position repeatability of the MWDPW, the conditions that generate the initial tension of each pulley must be determined. The initial tension is a function of the normal force applied to the pressure roller. Therefore, the aim here is to find the optimal number of pressure rollers and pressure forces through experiments under various conditions.

As shown in Fig. 28, the experiment is conducted by comparing cases with one and two pressure rollers. The experimental results are listed in Table 3. The experimental results show that higher pressure repeatability can be achieved when

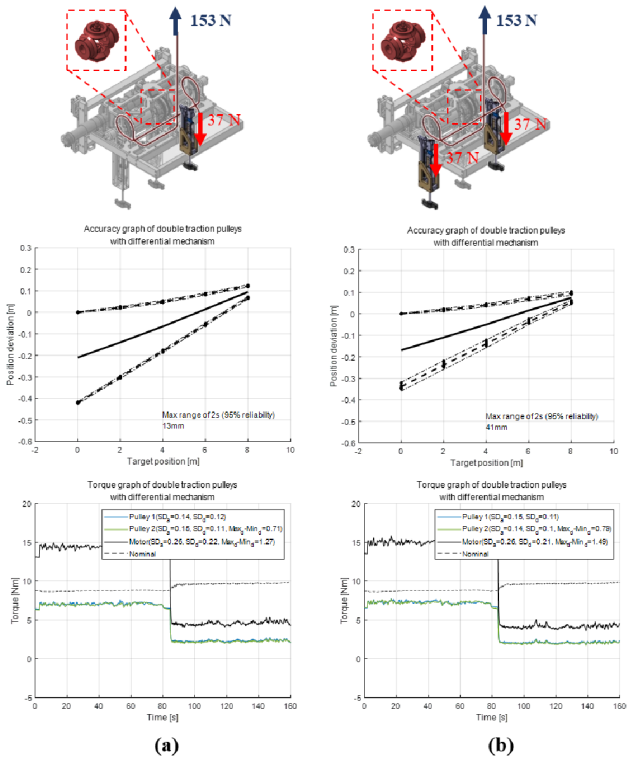

FIGURE 28. Experimental results of position repeatability and torque distribution with (a) 1 EA pressure roller and (b) 2 EA pressure roller.

TABLE 3. Position repeatability and standard deviation of torque with 1 ea and 2 ea pressure roller.

	1 EA pressure roller		2 EA pressure roller	
Repeatability [mm] (Maximum range of 2s)	13 (▼62%)		41	
Standard deviation of torque	3rd pulley	Motor	3rd pulley	Motor
	0.57 (▼28%)	1.07 (▼28%)	0.79	1.49

one pressure roller presses the traction pulley 1. This corresponds to the assumption that the torque distribution applied to each traction pulley must be more uniform in order to obtain better repeatability. In other words, when there is one pressure roller, the standard deviation of the torque is 28% lower, and as a result, the repeatability improves by 62%.

Lower repeatability with two pressure rollers can be considered as an additional pressure roller disturbing the torque distribution. If the payload is constant, then the tension at the fixed end and the tension at the free end are constant. Therefore, the tension at the beginning and end of the winch is always the same. However, the tension distribution inside the winch can be different. A change in the rope tension changes the length of the rope in the winch via distributing the tension by varying the rotation angle of the left and right pulleys through the differential gear mechanism. Applying a normal force to traction pulley 3 through a pressure roller changes the area where the rope slips. Therefore, the torque distribution of the differential gear mechanism is not constant, which worsens the repeatability. As a result, an optimal condition exists when there is one pressure roller.

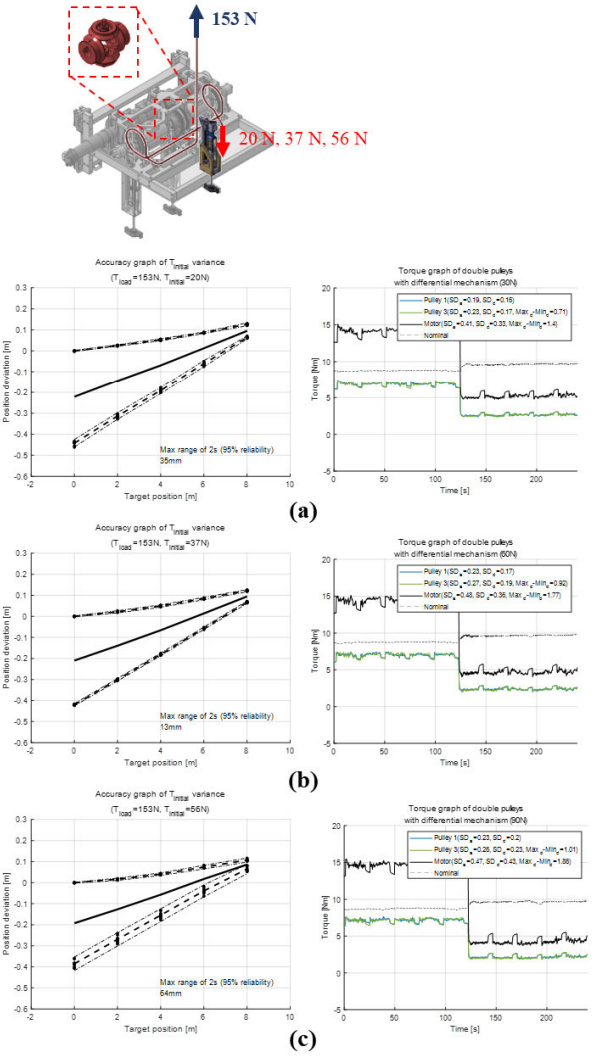

FIGURE 29. Experimental results of position repeatability and torque distribution with normal force of (a) 20 N, (b) 37 N, and (c) 56 N of pressure roller.

Depending on the normal force of the pressure roller, the rope tension when entering the winch from the free end can be expected to vary. However, owing to the nonlinear properties of synthetic fiber ropes, it is difficult to obtain the coefficient of kinetic friction between the wedge-shaped pulley and the rope. Therefore, as shown in Fig. 29, the position repeatability is measured for three cases where the normal force of the pressure roller is different. The experimental results are listed in Table 4, and the torque applied to each pulley is shown in Fig. 29.

The experimental results showed that the position repeatability is highest when the normal force applied to traction

TABLE 4. Position repeatability and standard deviation of torque with normal force of (a) 20 N, (b) 37 N, and (c) 56 N of pressure roller.

Normal force	20 N		37 N		56 N	
Repeatability [mm] (Maximum range of 2s)	35		13		64	
Standard deviation of torque	3rd pulley	Motor	3rd pulley	Motor	3rd pulley	Motor
	0.17	0.33	0.19	0.36	0.23	0.43

pulley 1 is 37 N. The normal force is related to the rope tension at the free end. However, a higher normal force is not more effective, and the differential gear mechanism can be operated ideally only when the proper loading tension and free-end tension are maintained. Therefore, through the position repeatability test in Section 4.2, the optimum design parameter of the final MWDPW was determined to be one pressure roller and 37 N of normal force.

V. EXPERIMENT AND DISCUSSION

The proposed MWDPW is developed for use in various kinds of climbing robots and gondolas. It is very important to maintain constant position repeatability for various payloads. Therefore, two verification experiments are conducted. First, an experiment is conducted to verify the effect of the torque distribution performance of the differential mechanism demonstrated in Section 3 on the position repeatability. A second experiment is conducted to verify that high position repeatability is maintained under various payloads when the optimal parameters obtained in Section 4 are applied.

The comparative experiments are conducted to confirm the effectiveness of the differential mechanism. Numerous numbers of capstan-winch-type products have been developed because a capstan winch can generate a large traction force from a small initial force. The general method to amplify the traction force is to increase the angle of the winding rope around the capstan drum or pulleys. The actual traction force generated from the pulleys can be measured with torque sensors. The actual effectiveness of a multipulley or capstan winch can be verified with this comparative experiment.

The result graphs of the comparative experiment are shown in Fig. 30. The differential mechanism case shows much better accuracy and repeatability performance than the rigid case. The maximum range of the 2*s* region of the differential case is 70% shorter than that of the rigid case. The main reason is the various changes in torque generated by the pulley, as shown in the torque graph of Fig. 30(a). There is no constant torque region in this graph. The torques of the three pulleys and the driving motor constantly change and do not settle at specific values. The torque graph of the differential case in Fig. 30(b) shows a relatively constant value.

The torques of the first and third pulleys have almost the same value because of the differential mechanism.

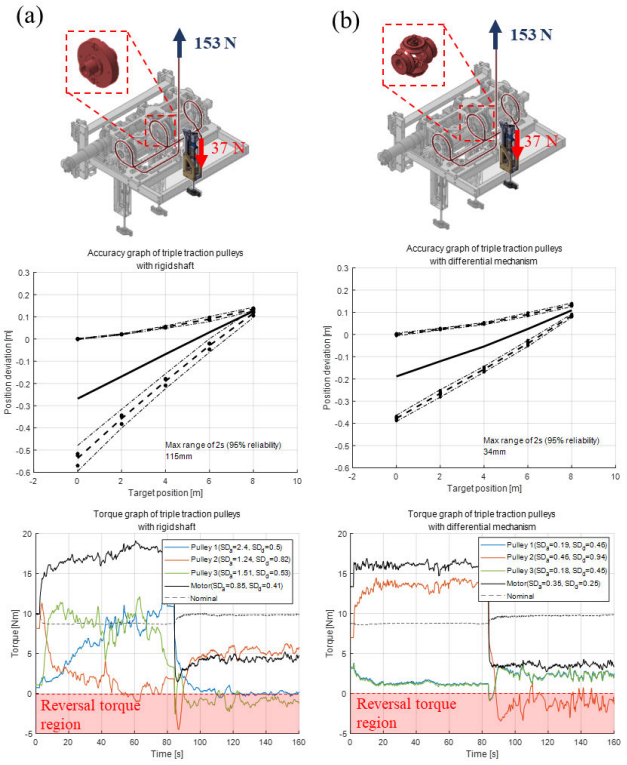

FIGURE 30. Experimental results of position repeatability with (a) rigid shaft and (b) differential mechanism cases.

A continuously changing torque means a continuous change amplification ratio of tension at each pulley. The amplification ratio of tension at the third pulley affects the actual descending distance. Therefore, a continuous changing torque of a pulley causes bad repeatability of the winch position. The changing torque of the driving motor also worsens the repeatability because it makes it difficult for the motor controller to follow the position precisely. Table 5 shows the better performance of the differential case.

TABLE 5. Position repeatability and standard deviation of torque between rigid shaft and differential mechanism cases.

	Rigid shaft case		Differential mechanism case	
Repeatability [mm] (Maximum range of 2s)	115		34 (▼70%)	
Standard deviation in descending motion	3rd pulley	Motor	3rd pulley	Motor
	0.53	0.41	0.45 (▼15%)	0.25 (▼39%)

Both cases have a reversal torque region during a descending motion. An effective torque direction should always be positive. A negative torque is useless for the winch mechanism to produce a traction force. The negative torque produces only internal frictional forces of the winch system, so the rest pulley should cover that force to generate enough traction. The second pulley in the rigid case in Fig. 30(a)

records a higher torque than that of the driving motor to compensate for the negative torque of the third pulley.

The comparative experiment shows that the general capstan winch mechanism is insufficient. The traction force was only generated in the small region on the traction surface, especially during a descending motion.

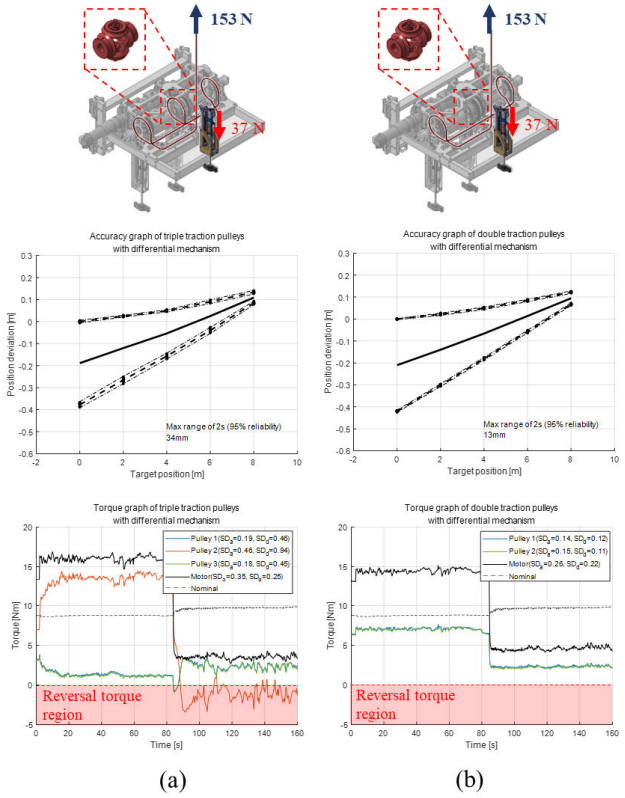

FIGURE 31. Experimental results of position repeatability with (a) triple winding rope and (b) double winding rope.

The effect of the winding rope method is verified with a comparative experiment in the differential mechanism case. The reference case is a triple winding rope around the winch, as shown in Fig. 30(b) and Fig. 31(a). The resulting graph shows that the double winding rope method has much better repeatability and maintains specific torque values of the pulley and motor. The position repeatability of the triple winding rope case is enhanced by 62% over the double winding rope case, as shown in Table 6. The torque of the first and second pulleys maintains half the value of the driving motor, which means that the differential mechanism activates properly when distributing the torque difference between the first and second pulleys. The first and second pulleys contribute equally to generating the total traction force. There is no reversal torque value shown in the torque graph of Fig. 31(b).

The triple winding rope case has the worst performance because the second pulley of that case disturbs the torque distribution of the differential mechanism. The differential

TABLE 6. Position repeatability and standard deviation of torque between rigid shaft and differential mechanism cases.

	Triple winding rope case		Double winding rope case	
Repeatability [mm] (Maximum range of 2s)	34		13 (▼62%)	
Standard deviation	3rd pulley	Motor	3rd pulley	Motor
	0.45	0.25	0.11 (▼76%)	0.22 (▼12%)

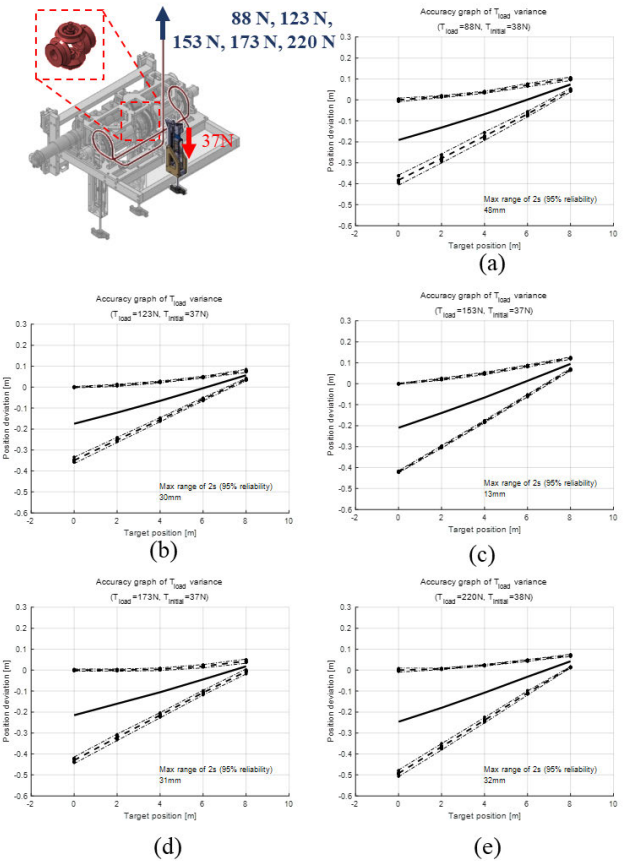

FIGURE 32. Experimental results of position repeatability with various payloads: (a) 88 N, (b) 123 N, (c) 153 N, (d) 173 N, and (e) 220 N.

mechanism can distribute the torques to the first and third pulleys but not to all three pulleys.

The best case is the differential mechanism with a double winding rope and single pressure roller, as shown in Table 6. A winch with this mechanism combination can be exposed to various payloads. The experimental results for various payloads are shown in Fig. 32 and Table 7. The repeatability becomes worse when the payload is lower or higher than that of the best case. As mentioned previously, proper force of the pressure roller is essential to achieve good repeatability. However, suitable forces according to various payloads cannot be applied to the pressure roller because that force is fixed.

TABLE 7. Position repeatability of MWDPW with optimized design parameter.

	T_{load} [N]				
	88	123	153	173	220
Repeatability [mm]	48	30	13	31	32

Therefore, deviations owing to different payloads should be overcome by the controller.

VI. CONCLUSION

This study proposed a winch mechanism with high position repeatability that uses synthetic fiber ropes. Multiple winding pulleys are used to achieve the target payload, and a differential gear mechanism is used to increase the durability of the winch and improve the positioning performance by equally distributing the torques applied to each of the pulleys. In order to select the optimal winch combination, the tension distribution is analyzed using the capstan equation, and the differential gear principle and is validated through experiments. This proves that optimum tension distribution is possible when connecting two pulleys with a differential gear mechanism. In addition, it is shown that the combination can maximize winch durability and increase the position repeatability by minimizing ineffective rope slip.

Experiments were conducted to optimize the design parameters of the winch in order to maximize position repeatability for the selected winch mechanism. First, a standard criterion for measuring the position repeatability of the winch was designed according to the ISO standards. Experiments showed that the use of one pressure roller for the traction pulley at the free end improved the repeatability by 62% compared to two pressure rollers. It was also shown that the optimum position repeatability could be achieved when the pressure of the pressure roller is 37 N. Extensive experiments were conducted to test the performance of the winch mechanism using a test bench. Reciprocating experiments were carried out for various payloads, and a position repeatability within 50 mm (0.5%) was achieved even with a 10-m reciprocating motion.

ACKNOWLEDGMENT

(Sungkeun Yoo and Taegyun Kim contributed equally to this work.)

REFERENCES

[1] Manntech, Mammendorf, Germany. *Auto Facade Cleaning*. Accessed: Mar. 20, 2020. [Online]. Available: http://www.koreamanntech.com/products/products05.htm

[2] T. Akinfiev, M. Armada, and S. Nabulsi, "Climbing cleaning robot for vertical surfaces," *Ind. Robot, Int. J.*, vol. 36, no. 4, pp. 352–357, Jun. 2009, doi: 10.1108/01439910910957110.

[3] S. Yoo, I. Joo, J. Hong, C. Park, J. Kim, H. S. Kim, and T. Seo, "Unmanned high-rise façade cleaning robot implemented on a gondola: Field test on 000-building in Korea," *IEEE Access*, vol. 7, pp. 30174–30184, 2019, doi: 10.1109/ACCESS.2019.2902386.

[4] Kite Robotics, Enschede, The Netherlands. *Kite Robotics Window Cleaning Robots*. Accessed: Mar. 20, 2020. [Online]. Available: https://www.kiterobotics.com

[5] N. Imaoka, S.-G. Roh, N. Yusuke, and S. Hirose, "SkyScraper-I: Tethered whole windows cleaning robot," in *Proc. IEEE/RSJ Int. Conf. Intell. Robots Syst.*, Taipei, Taiwan, Oct. 2010, pp. 5460–5465, doi: 10.1109/iros.2010.5649537.

[6] D. Wang, J. Ahn, J. Jung, J.-A. Seon, J.-O. Park, S. Y. Ko, and S. Park, "Winch-integrated mobile end-effector for a cable-driven parallel robot with auto-installation," *Int. J. Control, Automat. Syst.*, vol. 15, no. 5, pp. 2355–2363, Oct. 2017, doi: 10.1007/s12555-016-0398-7.

[7] Wall Robotics, Espoo, Finland. *Full Self Cleaning Robot From Wall Robotics*. Accessed: Mar. 20, 2020. [Online]. Available: https://www.wallrobotic.com

[8] IPC Eagle, USA. *HighRise Professional Window Cleaning System*. Accessed: Mar. 20, 2020. [Online]. Available: http://www.ipcworldwide.com/us/product/highrise-automatic-window-cleaning-system/

[9] K. Seo, S. Cho, T. Kim, J. Kim, and H. S. Kim, "Design and stability analysis of a novel wall-climbing robotic platform (ROPE RIDE)," *Mechanism Mach. Theory*, vol. 70, pp. 189–208, Dec. 2013, doi: 10.1016/j.mechmachtheory.2013.07.012.

[10] T. Kim, Y. Jeon, S. Yoo, K. Kim, H. S. Kim, and J. Kim, "Development of a wall-climbing platform with modularized wall-cleaning units," *Automat. Construct.*, vol. 83, pp. 1–18, Nov. 2017, doi: 10.1016/j.autcon.2017.07.004.

[11] O. Baser and E. I. Konukseven, "Theoretical and experimental determination of capstan drive slip error," *Mechanism Mach. Theory*, vol. 45, no. 6, pp. 815–827, Jun. 2010, doi: 10.1016/j.mechmachtheory.2009.10.013.

[12] F. Anderson and O. Ryesvej, "Capstan winch, particularly for sailing boats," U.S. Patent 4 595 173, Aug. 23, 1986.

[13] N. Ball, T. Fofonoff, B. Schmid, and D. Walker, "Powered rope ascender and portable rope pulling device," U.S. Patent 7 261 278, Aug. 28, 2007.

[14] M. S. Shafi, J. Lu, Z. Song, and Y. Fu, "Design and tension control of double drum winch system for deep-sea exploration equipment," in *Proc. 5th Int. Conf. Inf. Eng. Mech. Mater.*, Huhhot, China, 2015, pp. 1474–1480, doi: 10.2991/icimm-15.2015.269.

[15] J. Werkmeister and A. Slocum, "Theoretical and experimental determination of capstan drive stiffness," *Precis. Eng.*, vol. 31, no. 1, pp. 55–67, Jan. 2007, doi: 10.1016/j.precisioneng.2006.03.001.

[16] S. R. Torben, P. Ingeberg, Ø. Bunes, S. Bull, J. Paterson, and D. Davidson, "Fiber rope deployment system for ultradeepwater installations," in *Proc. Offshore Technol. Conf.*, Houston, TX, USA, 2007, doi: 10.4043/18932-MS.

[17] M. J. Leamy and T. M. Wasfy, "Analysis of belt-driven mechanics using a creep-rate-dependent friction law," *J. Appl. Mech.*, vol. 69, no. 6, pp. 763–771, Nov. 2002, doi: 10.1115/1.1488663.

[18] L. Kong and R. G. Parker, "Microslip friction in flat belt drives," *Proc. Inst. Mech. Eng., C, J. Mech. Eng. Sci.*, vol. 219, no. 10, pp. 1097–1106, 2005, doi: 10.1243/095440605X31959.

[19] S. E. Bechtel, S. Vohra, and K. I. Jacob, "Contrasting the predictions for Coulomb and creep-rate-dependent friction in the modeling of fiber-draw processes," *J. Appl. Mech.*, vol. 79, no. 6, pp. 1001–1004, Nov. 2012, doi: 10.1115/1.4005532.

[20] *Test Code for Machine Tools—Part 2: Determination of Accuracy and Repeatability of Positioning of Numerically Controlled Axes*, ISO Standard ISO 230-2:2014, 2014.

SUNGKEUN YOO received the B.S. degree in mechanical and aerospace engineering from Seoul National University, in 2014, where he is currently pursuing the Ph.D. degree in mechanical engineering. His research interest includes robot mechanism design.

TAEGYUN KIM received the B.S. and Ph.D. degrees in mechanical and aerospace engineering from Seoul National University, Seoul, South Korea, in 2011 and 2017, respectively.

He is currently an Assistant Professor with the School of Mechanical Engineering, Yeungnam University, Gyeongsan, South Korea. His research interests include robot mechanism design, modeling, and control.

MYOUNGJAE SEO received the B.S. degree in mechanical engineering from Hanyang University, in 2019, where he is currently pursuing the M.S. degree. His research interests include robot design, control, and optimization.

JOOHYUN OH received the B.S. degree from the School of Mechanical Engineering, Hanyang University, South Korea, where he is currently pursuing the M.S. degree. His research interests include mechanism and linkage design and its application to clamping device.

JONGWON KIM received the B.S. degree in mechanical engineering from Seoul National University, South Korea, in 1978, the M.S. degree in mechanical and aerospace engineering from the Korea Advanced Institute of Science and Technology (KAIST), South Korea, in 1980, and the Ph.D. degree in mechanical engineering from the University of Wisconsin-Madison, USA, in 1987. He is currently a Professor with the School of Mechanical and Aerospace Engineering, Seoul National University. His current research interests include parallel mechanisms, Taguchi methodology, and field robots.

HWA SOO KIM (Member, IEEE) received the B.S. and Ph.D. degrees in mechanical engineering from Seoul National University, South Korea, in 2000 and 2006, respectively. He is currently an Associate Professor with the Department of Mechanical System Engineering, Kyonggi University. His current research interests include design, modeling, and control of various mobile platforms for wall-cleaning, and stair-climbing.

TAEWON SEO (Member, IEEE) received the B.S. and Ph.D. degrees from the School of Mechanical and Aerospace Engineering, Seoul National University, Seoul, South Korea, in 2003 and 2008, respectively.

He is currently an Associate professor with the School of Mechanical Engineering, Hanyang University, Seoul. His research interests include robot design, analysis, control, optimization, and planning. He was a recipient of the Best Paper Award of the IEEE/ASME Transactions on Mechatronics, in 2014. He serves as a Technical Editor for the IEEE/ASME TRANSACTIONS ON MECHATRONICS. He also serves as an Associate Editor for the IEEE ROBOTICS AND AUTOMATION LETTERS and *Intelligent Service Robotics*.